Journal of Experimental Botany, Vol. 67, No. 5 pp. 1461–1475, 2016
doi:10.1093/jxb/erv538 Advance Access publication 17 December 2015

RESEARCH PAPER

The Hippo/STE20 homolog SIK1 interacts with MOB1 to regulate cell proliferation and cell expansion in Arabidopsis

Jie Xiong, Xuefei Cui, Xiangrong Yuan, Xiulian Yu, Jialei Sun and Qingqiu Gong*

Tianjin Key Laboratory of Protein Sciences, Department of Plant Biology and Ecology, College of Life Sciences, Nankai University, Tianjin 300071, China

* Correspondence: gongq@nankai.edu.cn

Received 3 July 2015; Accepted 26 November 2015

Editor: James Murray, Cardiff University

Abstract

Multicellular organisms co-ordinate cell proliferation and cell expansion to maintain organ growth. In animals, the Hippo tumor suppressor pathway is a master regulator of organ size. Central to this pathway is a kinase cascade composed of Hippo and Warts, and their activating partners Salvador and Mob1/Mats. In plants, the Mob1/Mats homolog MOB1A has been characterized as a regulator of cell proliferation and sporogenesis. Nonetheless, no Hippo homologs have been identified. Here we show that the Arabidopsis serine/threonine kinase 1 (SIK1) is a Hippo homolog, and that it interacts with MOB1A to control organ size. SIK1 complements the function of yeast Ste20 in bud site selection and mitotic exit. The *sik1* null mutant is dwarf with reduced cell numbers, endoreduplication, and cell expansion. A yeast two-hybrid screen identified Mob1/Mats homologs MOB1A and MOB1B as SIK1-interacting partners. The interaction between SIK1 and MOB1 was found to be mediated by an N-terminal domain of SIK1 and was further confirmed by bimolecular fluorescence complementation. Interestingly, *sik1 mob1a* is arrested at the seedling stage, and overexpression of neither *SIK1* in *mob1a* nor *MOB1A* in *sik1* can rescue the dwarf phenotypes, suggesting that SIK1 and MOB1 may be components of a larger protein complex. Our results pave the way for constructing a complete Hippo pathway that controls organ growth in higher plants.

Key words: *Arabidopsis thaliana*, cell division, cell expansion, Hippo, MOB1, organ growth, SIK1, STE20.

Introduction

In a single plant species, mature leaves and flowers generally have determinate sizes. Although environmental factors influence the process, it is the genetic program that co-ordinates cell proliferation and cell expansion, thus determining the final organ sizes (Krizek, 2009; Gonzalez *et al.*, 2012; Powell and Lenhard, 2012; Hepworth and Lenhard, 2014). Many key players in plant organ size control have plant-specific functions. These include transcription factor gene families *Growth-Regulating Factor* (*GRF*) (Omidbakhshfard *et al.*, 2015), *TEOSINTEBRANCHED1/CYCLOIDEA/PCF* (*TCP*) (Martin-Trillo and Cubas, 2010), and *AINTEGUMENTA* (*ANT*) (Krizek, 1999; Mizukami and Fischer, 2000), the auxin-inducible gene *ARGOS* and its homologs *ARGOS-LIKE* (*ARL*) and *ORGAN SIZE RELATED1* (*OSR1*) (Hu *et al.*, 2003, 2006; Feng *et al.*, 2011), the *AUXIN RESPONSE FACTOR ARF2* (Schruff *et al.*, 2006), the ubiquitin receptor *DA1* (Li *et al.*, 2008), the E3 ligases *DA2* (Xia *et al.*, 2013) and *ENHANCER OF DA1 (EOD1)/BIG BROTHER*

(Disch *et al.*, 2006), *UBIQUITIN-SPECIFIC PROTEASE 15* (*UBP15*) (Du *et al.*, 2014), etc. Others play roles in more general processes such as cell cycle control and mitotic exit (Blomme *et al.*, 2014), cell expansion (Cho and Cosgrove, 2000; Zenoni *et al.*, 2011' Goh *et al.*, 2012), proteasome activity (Kurepa *et al.*, 2009; Sonoda *et al.*, 2009), etc. TOR (target of rapamycin) and TCTP (translationally controlled tumor protein), components of the TOR pathway, have also been shown to regulate organ growth as in animals (Deprost *et al.*, 2007; Brioudes *et al.*, 2010; Xiong *et al.*, 2013).

In the past few years, enormous efforts have been made in integrating the known regulators of plant growth (Sablowski and Carnier Dornelas, 2014; Wuyts *et al.*, 2015). Not only have regulatory networks been constructed at the cellular and organismal levels, but interactions between plants and their environments have been taken into account. In a systems biology era, identification and characterization of new growth control components are still of great importance, as they can be new nodes and missing links in the models and networks.

The STErile 20 (STE20)-like kinases are a family of evolutionarily conserved serine/threonine protein kinases (Dan *et al.*, 2001). The founder member of the family, Ste20 from budding yeast (*Saccharomyces cerevisiae*), was initially identified through a genetic screen for mating defects (Bardwell, 2005). Studies have since integrated Ste20 into other mitogen-activated protein kinase (MAPK) signaling cascades that mediate invasive growth (Roberts and Fink, 1994), osmosensing (Raitt *et al.*, 2000), bud site selection (Sheu *et al.*, 2000), mitotic exit (Hofken and Schiebel, 2002), and vacuole inheritance (Bartholomew and Hardy, 2009), among others. In general, the signaling is initiated by the binding of the Rho GTPase Cdc42 to Ste20 (Lamson *et al.*, 2002), which in turn is recruited to the plasma membrane (PM) by the G-protein β-subunit Ste4 (Leeuw *et al.*, 1998). The activated Ste20 then phosphorylates Ste11, a MAPK kinase kinase (MAP3K) (Drogen *et al.*, 2000), which phosphorylates downstream components such as Ste7 and Pbs2 (Harris *et al.*, 2001). Moreover, Ste20 acts as a histone kinase to promote apoptosis (Ahn *et al.*, 2005), and is a negative regulator of sterol uptake (Lin *et al.*, 2009).

Based on their domain structures, the STE20-like kinase family is divided into the p21-activated kinases (PAKs) and the germinal center kinases (GCKs) (Boyce and Andrianopoulos, 2011). PAKs have a p21 GTPase-binding domain (PBD)/Cdc42/Rac interactive binding motif (CRIB) at their N-termini and a kinase domain at their C-termini (Eswaran *et al.*, 2008). They are further divided into PAK-I and PAK-II subfamilies. PAK-Is (including ScSte20) are activated by binding to GTP-bound small G-proteins Cdc42 and Rac (p21). PAK-IIs have higher basal level kinase activity, and do not require GTPase binding to be activated (Eswaran *et al.*, 2008). PAKs are generally involved in cytoskeletal rearrangement, cellular morphogenesis, and survival (Harvey and Tapon, 2007). GCKs have a kinase domain at their N-terminus and lack GTPase-binding domains, and are subdivided into GCK-I–GCK-VIII. Although GCK functions have been implicated in JNK, p38, and NF-κB signaling pathways, it was the identification of the *Drosophila melanogaster* GCK Hippo (Hpo) (Harvey *et al.*, 2003; Jia *et al.*, 2003; Pantalacci *et al.*, 2003; Udan *et al.*, 2003; Wu *et al.*, 2003), along with its mammalian homologs MST1 and MST2, as tumor suppressors, and further establishment of the Salvador–Warts–Hippo (SWH) pathway as a core mechanism co-ordinately controlling cell proliferation and apoptosis (Harvey and Tapon, 2007; Pan, 2010; Rawat and Chernoff, 2015), that have induced general interest. The SWH/Hippo pathway has four core components: the protein kinases Hpo and Warts (Wts), and two scaffold proteins Salvador (Sav) and Mob1 as a tumor suppressor (Mats). Basically, Hpo, in conjunction with Sav, phosphorylates Mats and Wts to activate them. Activated Wts then phosphorylates a transcriptional coactivator (and an oncogene) Yes-associated protein (Yap), leading to its cytoplasmic sequestration and inactivation, and thus suppresses cell proliferation and induces apoptosis (Rawat and Chernoff, 2015).

So far, whether the SWH/Hippo pathway is conserved between animals and plants remains unknown. Among the four core components, only Mats homologs have been identified in plants. In a survey on potential cytokinesis genes, Mob1 was shown to localize to the nucleus in tobacco cells and in transgenic Arabidopsis (Van Damme *et al.*, 2004). Subsequently, MOB homologs have been characterized in alfalfa (Citterio *et al.*, 2005, 2006) and Arabidopsis (Galla *et al.*, 2011). RNAi of Arabidopsis *MOB1* leads to reduced cell proliferation and impaired sporogenesis and gametogenesis (Galla *et al.*, 2011). A recent study further suggested the involvement of MOB1A in tissue patterning (Pinosa *et al.*, 2013). Obviously, finding the kinase with which the scaffold protein works is a prerequisite for constructing a potential plant Hippo pathway.

Here we report the putative serine/threonine kinase (SIK1) as a STE20 and Hippo homolog in Arabidopsis. Previously, SIK1 has been predicted as a MAPK kinase kinase kinase (MAP4K) and STE20-like human kinase (SLK) (Jonak *et al.*, 2002; Karpov *et al.*, 2010). It has also been reported to have serine/threonine kinase activity in a large-scale study (Nemoto *et al.*, 2011). Nevertheless, the *in vivo* function of SIK1 remains elusive. We first complemented the yeast *ste20Δ* mutant with SIK1. Then, through phenotypic analysis of the *sik1* null mutant, we demonstrated a role for SIK1 as a regulator of both cell proliferation and cell expansion. Furthermore, through a yeast two-hybrid (Y2H) screen, we identified the two Arabidopsis MOBs, AtMOB1A and AtMOB1B, as SIK1-interacting proteins. The interactions were further confirmed to be mediated mainly by an N-terminal domain of SIK1. Interestingly, MOB1–SIK1 interaction led to translocation of SIK1 to the nucleus, and the N-terminal domain of SIK1 appeared to be responsible for the nuclear localization of SIK1. Finally, genetic analyses suggested that SIK1 and MOB1 may be constituents of a larger protein complex. To our knowledge, this is the first study on a STE20-like kinase in Arabidopsis, which lays a foundation for future construction of a complete Hippo pathway of higher plants.

Materials and methods

All experiments were performed at least in triplicate. Primers used in this study are listed in Supplementary Table S1 at *JXB* online.

Accession numbers

SIK1, At1g69220; Mob1A, At5g45550; Mob1B, At4g19045.

Plant materials and growth conditions

The *sik1-1* (*SALK_051369*), *sik1-2* (*SALK_010630*), *sik1-3* (*SALK_046158*), *sik1-4* (*SAIL_636_C05, CS875528*), *mob1a-1* (*GABI_719G04, CS469004*), and *mob1b-1* (*SALK_062070*) lines and the *pSAT1-nEYFP-N1* and *pSAT1-cEYFP-N1* vectors were obtained from the Arabidopsis Biological Resource Center (ABRC). *pCycB1;1:GUS* was a gift from Dr Peter Doerner. All mutants were verified by genomic PCR and reverse transcription–PCR (RT–PCR). *Nicotiana benthamiana* seeds were a gift from Dr Yule Liu.

Generally, Arabidopsis (ecotype columbia-0) seeds were surface-sterilized with 75% ethanol for 5 min, 100% ethanol for 1 min, rinsed with ddH_2O five times, then stratified at 4 °C for 2 d before plating on half-strength Murashige and Skoog (1/2 MS) medium (Sigma-Aldrich, USA) containing 0.8% (w/v) agar, 1% (w/v) sucrose, pH 5.7. The plants were then grown at 16 h (22 °C)/8 h (18 °C) with a photosynthetic photon flux density at 90 μE m^{-2} s^{-1}. Soil-grown plants were kept under the same conditions.

Phenotypes of seedlings were captured with a stereoscope (Leica 165FC, Germany) equipped with a CCD camera, or a scanner (Epson Perfection V33). Soil-grown plants were photographed with a digital camera (Canon Powershot A800).

Constructs and transgenic plants

SIK1 has two splicing variants which differ in 81 nucleotides at their N-termini (Supplementary Fig. S1). Quantitative real-time PCR (Q-RT-PCR) showed that *At1g69220.1* (2511 bp) is the major form of the *SIK1* transcript in most organs (Supplementary Fig. S1). Thus, all constructs in this study were made with *At1g69220.1*.

For the *pUBQ10:GFP-SIK1* construct, *SIK1* full-length cDNA was PCR-amplified and then inserted in-frame behind green fluorescent protein (GFP) of a modified *pCAMBIA1302* (35S promoter replaced by *pUBQ10*) by homologous recombination (CloneEZ kit, GenScript, China).

35S:YFP-Myc-Mob1A: *Mob1A* cDNA was PCR-amplified and inserted in-frame behind yellow fluorescent protein (YFP)-Myc of a modified *pCAMBIA1302* vector by homologous recombination.

For *pSIK1:GUS* and *pSIK1:SIK1-GUS*, the full-length intergenic region between *At1g69230* and *At1g69220* (*SIK1*), a 417 bp fragment upstream of ATG of *SIK1*, was PCR-amplified and inserted between the *Pst*I and *Nco*I sites of *pCAMBIA1301*. Then *SIK1* cDNA was inserted in-frame before β-glucuronidase (GUS) by homologous recombination.

For yeast two-hybrid verification, cDNAs of full-length *SIK1* and fragments thereof (N1, N2, N, C1) and full-length *MOB1A* and *MOB1B* were cloned into *pGADT7* (AD) and *pGBKT7* (BD) vectors by homologous recombination. Bimolecular fluorescence complementation (BiFC) constructs were made similarly with *pSAT1-nEYFP-N1* and *pSAT1-cEYFP-N1* vectors.

All constructs were verified by DNA sequencing before being introduced into *Agrobacterium tumefaciens* (GV3101) for floral dipping (Clough and Bent, 1998). Primary transformants were selected by antibiotic resistance and further verified by PCR. *pCycB1;1:GUS* was introduced into *sik1-4* by crossing.

Gene expression analysis

RNA extraction, reverse transcription, RT–PCR, and Q-RT-PCR were performed as described (Xia *et al.*, 2012). To profile gene expression of the first and second leaves of 8-, 11-, and 14-day-old seedlings, leaves were dissected from the plant under a stereoscope (Leica 165FC, Germany) and placed in Trizol. A minimum of 200 leaves per replicate were harvested.

Histochemical GUS staining of homozygous T_3 transgenic lines harboring *pSIK1:GUS* and *pSIK1:SIK1-GUS* fusion genes, and *sik1-4*/*pCycB1;1:GUS* was done as described (Liu *et al.*, 2010).

Yeast complementation, yeast two-hybrid screen, and verification

The yeast strain TN124 (*MAT*a *leu2-3*,112 *trp1 ura3-52 pho8:. pho8A60 phol3::LEU2*) was used for complementation experiments. *ste20Δ* was generated by homologous recombination (replacing *STE20* with *URA3*), and *pRS414-ScSte20pmtr-SIK1* was constructed and introduced into *ste20Δ* by the standard lithium acetate (LiAc) transformation method as described (Xia *et al.*, 2012). Strains were confirmed by PCR. All strains were streaked out on plates with appropriate selection medium and grown at 30 ºC for 3 d. Cells from single colonies were then dispersed in liquid yeast extract/peptone/dextrose (YPD) medium for phase contrast microscopy (Leica DM2500, Germany).

The yeast strain AH109 (Clontech) was used for Y2H experiments. The Mate & Plate™ Library-Universal Arabidopsis (Normalized) (Clontech) was used for screening SIK1-interacting proteins (~6×10^6 transformants) following the manufacturer's instructions. Plasmids from >300 positive clones developed on –Trp–Leu–His plates were extracted for sequencing. Sequencing results were compared with TAIR10 transcripts with BLAST (https://www.arabidopsis.org/Blast/index.jsp) to obtain AGI numbers and annotations, which are listed in Supplementary Table S2.

To verify the interactions between SIK1 and MOB1s, yeast cells were first transformed with the BD constructs. Single colonies developed on –Trp plates were inoculated into liquid –Trp medium and grown at 30 ºC with constant shaking at 220 rpm to mid-logarithmic phase. A 5 ìl aliquot of liquid culture was dropped onto –Trp –His –Ade (TDO) plates for self-activation detection. Clones without self-activation activities were then transformed with AD constructs and grown on –Trp –Leu (DDO) plates. Colonies were inoculated into liquid DDO medium, grown to mid-log phase, dropped onto DDO, TDO, and –Trp –Leu –His –Ade (QDO) plates, and allowed to develop for 3 d before photographing.

Quantification of cell size and numbers

For root hair length measurement, primary roots from vertically grown, 7-day-old seedlings were photographed under a stereoscope (Leica 165FC, Germany). To measure root meristem size and cell number, 6-day-old seedlings were fixed with acetic acid/ethanol (3:1, v:v) for 4 h, then cleared with chloral hydrate/dH_2O/glycerol (8 g:3 ml:1 ml) for 4 h. Then the root tips were photographed with a CCD camera under a microscope with differential interference contrast (DIC) mode (Olympus DP72, Japan). To quantify petal growth parameters, freshly opened flowers were collected, and petals were detached, fixed for 10 min, and then cleared for 10 min before microscopic observation. To quantify leaf growth parameters, the fifth rosette leaves at 28 d post-germination were collected, fixed, and cleared until mostly transparent for microscopic observation.

All quantification was done with Image J (http://rsb.info.nih.gov/ij/), and statistical analysis (*F*-test, *t*-test) was done using Microsoft Excel 2010.

Measurement of nuclear DNA content of leaf cells by flow cytometry

Nuclei were extracted from the fifth rosette leaves of 28-day-old, soil-grown plants as described (Galbraith *et al.*, 1983). Nuclei were stained with 50 mg ml^{-1} propidium iodide and analyzed on a FACSAria II flow cytometer (BD, USA).

Transient transformation of tobacco leaves

Transient transformation was done as described (Liu *et al.*, 2005) on soil-grown, 4-week-old *N. benthamiana* leaves. After 2 d of inoculation, leaves were collected and cut into small squares for confocal microscopy.

Laser scanning confocal microscopy (LSCM)

Transiently transformed tobacco leaves (lower leaf epidermis) were incubated in 5% glycerol and scanned with a Leica SP5 (Leica, Germany).

Results

The Arabidopsis SIK1 *encodes a STE20-like kinase*

To look for possible STE20/Hippo homologs in Arabidopsis, we performed a BLASTP (Basic Local Alignment Tool for Proteins) search against the Arabidopsis protein database (TAIR10) with Ste20 from *S. cerevisiae* (YHL007C, AAA35039.1), Hippo from *D. melanogaster* (AAF57543.2), and Mst1 and Mst2 from *Homo sapiens* (AAA83254.1 and AAC50386.1). Among all Arabidopsis proteins, the putative serine/threonine kinase SIK1 (At1g69220) shares the highest homology with all four queries (identities=39%, positives=58% with Ste20; 51% and 68% with Hippo; 50% and 66% with Mst1; and 44% and 60% with Mst2).

A previous large-scale study had reported that SIK1 has serine/threonine autophosphorylation activity, thus confirming its molecular function as a protein kinase (Nemoto *et al.*, 2011). The kinase domain is at the center of the protein (amino acids 249–503) (Fig. 1A) and is well conserved with those of Hippo, Mst1, and Mst2 (Fig. 1B). However, SIK1 does not have any protein–protein interaction domains and motifs identified in Ste20, Hippo, or Msts (Fig. 1A; Supplementary Fig. S2). On the other hand, SIK1 is well conserved among land plants (NCBI protein cluster CLSN2689098, Fig. 1C).

Yeast complementation was done to see if SIK1 is an ortholog of Ste20. As reported (Sheu *et al.*, 2000; Hofken and Schiebel, 2002), *ste20Δ* cells are frequently irregular in shape and have defects in bud site selection and mitotic exit (Fig. 1D). Out of 131 budding cells, 45.8% had an abnormal budding pattern. In contrast, *ste20Δ* complemented with *pSte20:SIK1* looked no different from the background strain TN124 (Fig. 1D), with only 5.0% of cells showing an abnormal budding pattern (n=140), comparable with that of TN124 (4.3%, n=138). The phenotypic analysis indicated that SIK1 can complement Ste20 function in bud site selection and mitotic exit.

Our efforts to complement the *Drosophila hpo* mutant with SIK1 failed (data not shown), suggesting that a relatively large functional divergence exists between the plant and animal homologs.

SIK1 *is expressed in mature tissues and is post-transcriptionally regulated*

To gain insights into the physiological function of SIK1, tissue-specific expression of *SIK1* was first examined. *SIK1* mRNA can be detected in all organs by RT–PCR (Fig. 2A). Transgenic lines carrying *pSIK1:GUS* were generated using a 418 bp (–417 to +1) fragment—the full-length intergenic region— upstream of the *SIK1* start codon. Interestingly, *SIK1* promoter activity was relatively high in mature tissues and organs, such as hypocotyl of etiolated and light-grown

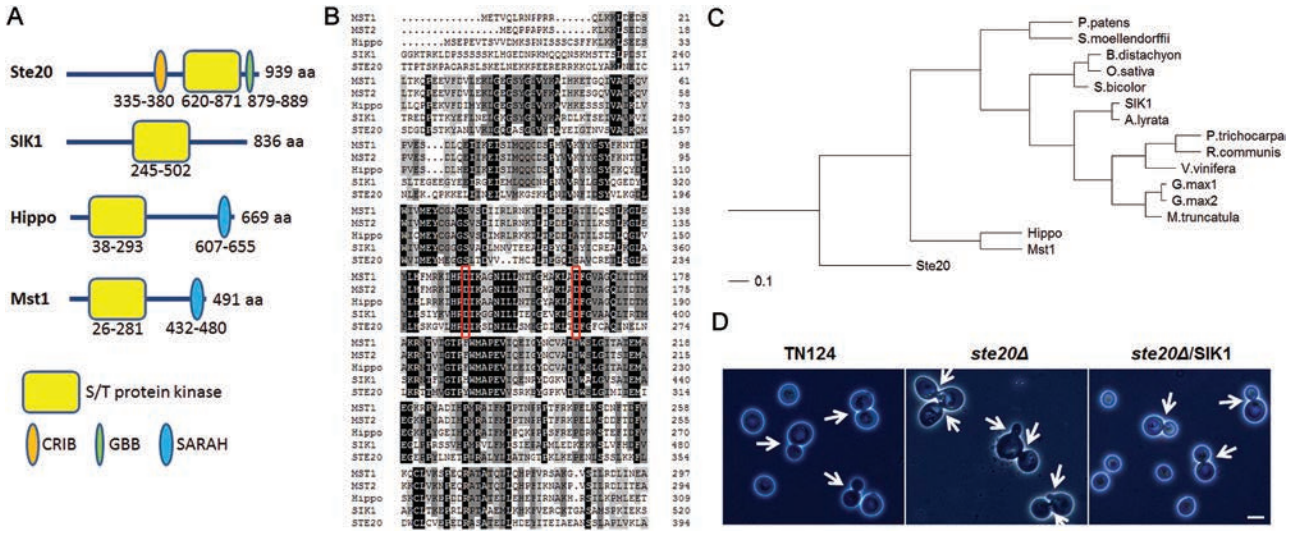

Fig. 1. Arabidopsis SIK1 is a Ste20 and Hippo homolog. (A) Schematic representation of the domain structure of Ste20 family proteins. The serine/threonine protein kinase domain and the domains that mediate protein–protein interaction (PPI), including the Cdc42/Rac interactive binding (CRIB) and G beta-binding (GBB) motif of Ste20, and the Sav/Rassf/Hpo (SARAH) domain of Hippo and Mst1, are shown. No PPI domain can be identified in SIK1. (B) Alignment of the Ste20 family proteins. The kinase domains are highly conserved. D371 and D389 of SIK1 are predicted active sites (boxes). (C) Phylogenetic tree of SIK1 homologs from selected land plants, with metazoan and yeast Ste20 homologs as outliers. The tree is constructed with Clustal W2-generated multiple sequence alignment of SIK1 homologs (NCBI protein cluster CLSN2689098, protein kinase domain-containing protein) using the Neighbor–Joining method and plotted in Treeview. (D) SIK1 restores abnormal budding phenotypes in *ste20*Δ. Yeast cells from the background strain TN124 and *ste20*Δ complemented with SIK1 (*ste20*Δ/SIK1) are normal in cell shape and budding site selection. *ste20*Δ cells are irregular in shape with an abnormal budding pattern. Arrows indicate budding sites. Scale bar=5 μm in (D). (This figure is available in colour at *JXB* online.)

3-day-old seedlings (Fig. 2B, C), fully expanded cotyledons (Fig. 2D), and the quiescent center and maturation zone of the primary root in 7-day-old seedlings (Fig. 2E-F). In 14-day-old plants, GUS activity was mainly detected in the cotyledons and the first pair of true leaves (Fig. 2G). In 28-day-old plants, the mature rosette leaves had strong GUS staining (Fig. 2H). Pollen of opened flowers is clearly stained (Fig. 2I–K). In contrast, less staining was observed in tissues that undergo cell division, such as young cotyledons (Fig. 2C), the division zone of the primary root (Fig. 2E), and developing young leaves (Fig. 2D, G, H).

We then generated a translational fusion of the *SIK1* cDNA with GUS under control of the SIK1 promoter, and obtained homozygous transgenic lines carrying *pSIK1:SIK1-GUS* (*SIK1:GUS*). In 10-day-old plants, GUS staining was detected in developed vascular tissues (Fig. 2L, N, P, Q), stipules of true leaves (Fig. 2 M–O; Supplementary Fig. S3), mature trichomes, and guard cells (Supplementary Fig. S3) in both *pSIK1:GUS* and *SIK1:GUS*. Staining of *SIK1:GUS* was restricted to smaller regions compared with *pSIK1:GUS* (Fig. 2L–S), suggesting the existence of post-transcriptional regulation of SIK1 protein. Indeed, we observed that transgenic lines carrying *35S:GFP-SIK1* had sizes comparable with the wild-type despite having higher *SIK1* mRNA levels (Supplementary Fig. S4).

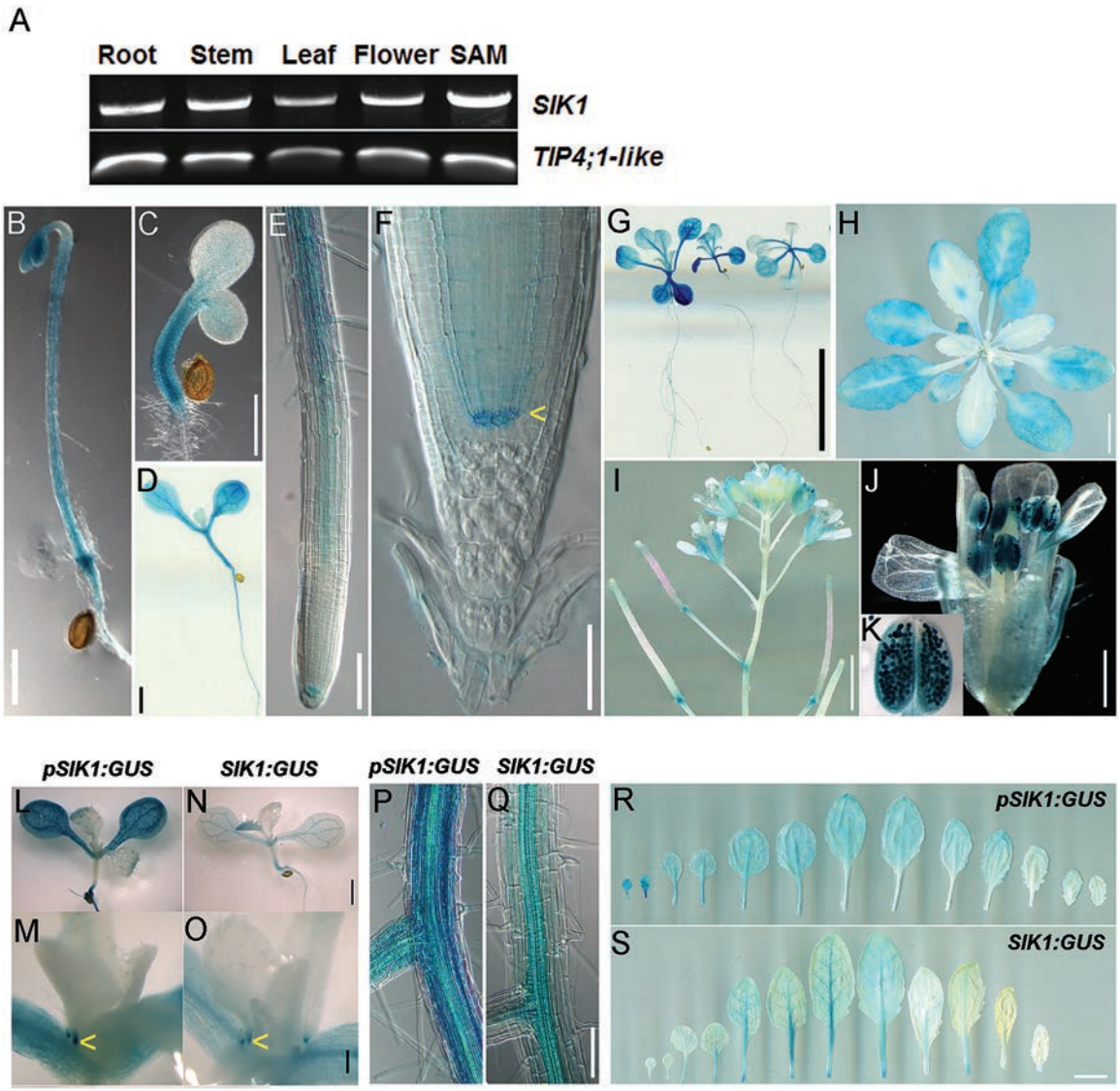

Fig. 2. Developmental expression and post-translational regulation of SIK1. (A) Semi-quantitative RT-PCR analysis of *SIK1* transcript in different organs. *TIP4;1-like* used as internal control. (B–K) Histochemical staining of *pSIK1:GUS* T3 homozygous plants. SIK1 promoter activity is detected in (B) 3-day-old etiolated seedlings, (C) 3-day-old light-grown seedlings, (D) 7-day-old seedlings, (E) primary root of 7-day-old seedlings, (F) quiescent center of the root apical meristem, (G) 14-day-old seedlings, (H) 4-week-old plants, (I) inflorescence, (J) opened flowers, and (K) pollen grains. (L–S) Comparison between expression of *SIK1* transcriptional and translational fusions. GUS activity in *SIK1:GUS* transgenic lines is further restricted compared with *pSIK1:GUS* lines in (L–Q) 10-day-old seedlings and (R, S) rosette leaves of 4-week-old plants. The arrows indicate the quiescent center in (F), and stipules of leaves one and two in (M) and (O). Scale bars=500 μm in (B), (C), (J); 1 mm in (D), (N); 100 μm in (E), (O), (Q); 50 μm in (F); 1 cm in (G), (H), (S); 5 mm in (I). (This figure is available in colour at *JXB* online.)

Growth of sik1 *mutants is retarded*

To analyze the physiological functions of SIK1 in Arabidopsis, T-DNA insertion lines were obtained from the ABRC (Sessions *et al.*, 2002; Alonso *et al.*, 2003) (Fig. 3A). Four homozygous lines were confirmed with PCR and RT–PCR. *sik1-4* (*SALK_051369*), *sik1-1* (*SALK_046158*), and *sik1-2* (*SAIL_636_C05,CS875528*) are null alleles, whereas *sik1-3* (*SALK_010630*), in which T-DNA is inserted in the seventh intron of *SIK1*, is a weak allele with a detectable level of *SIK1* mRNA (Fig. 3B). All alleles except for *sik1-3* appeared dwarf and were slow in growth compared with the wild type (Fig. 3C). Since *sik1-4* is the only allele in which a transcript for the kinase domain cannot be detected, our studies were carried out mainly with *sik1-4*.

To confirm further the causal relationship between the T-DNA insertion and the dwarf phenotype, a transgenic line carrying *pUBQ10:GFP-SIK1* was generated and crossed into *sik1-4* for complementation. RT–PCR confirmed the elevated *SIK1* mRNA level in the complementation line (Fig. 4A). Growth parameters of *sik1-4*, the complementation line, and the wild type were then documented and statistically analyzed. All *sik1* phenotypes, including short root, small rosette, reduced plant height, small flowers, siliques, and seeds, were restored to wild-type levels in the complementation line (Fig. 4B–K; Supplementary Table S3), confirming that the phenotypes were indeed caused by the T-DNA insertion in *sik1-4*.

Cell number, cell size, and the ploidy level are reduced in sik1-4

To see if the dwarf phenotype of *sik1* is a result of reduced cell proliferation or less cell expansion, cell number and cell size of the root apical meristem (RAM) of 7-day-old seedlings, the fifth rosette leaf of 4-week-old plants, and the petal of fully opened flowers were quantified in both *sik1-4* and the wild type, respectively. The length of the RAM (measured

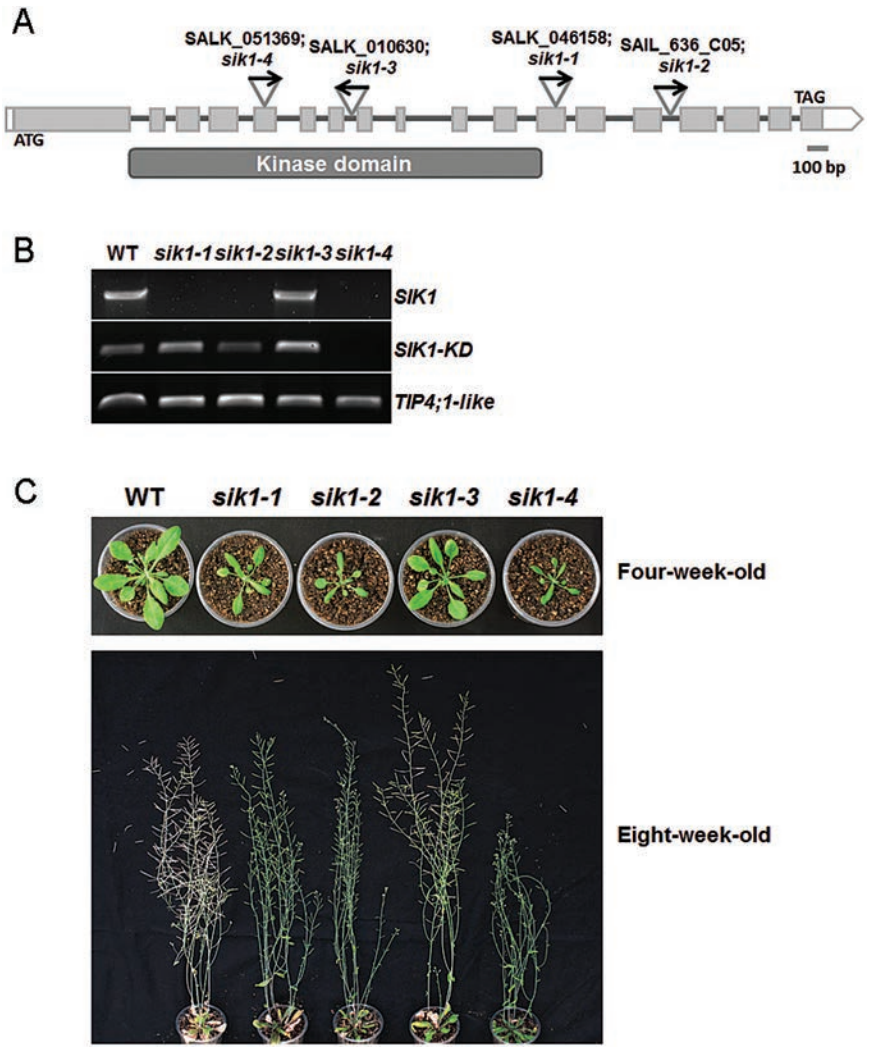

Fig. 3. The *sik1* null mutant has a dwarf phenotype. (A) *SIK1* gene structure and the T-DNA insertions. Exons, introns, and untranslated regions are represented by gray boxes, gray lines, and white boxes, respectively. Insertion positions of the T-DNA in the four alleles are shown. (B) *sik1-4* is a null allele. An mRNA fragment representing the kinase domain (KD; exons 2–12) can be detected in *sik1-1*, *sik1-2*, and *sik1-3*, but not in *sik1-4*. *sik1-3* is a knock-down allele, with the T-DNA inserted into the seventh intron. (C) Phenotypes of four alleles. The three null alleles are slow in growth compared with the wild type, with *sik1-4* having the most severe phenotypes. Diameter of pot=6.5 cm in (C). (This figure is available in colour at *JXB* online.)

from the quiescent center up to the beginning of the elongation zone) of *sik1-4* was reduced to 62% of that of the wild type, and protoderm cell number was 63% of that of the wild type (Fig. 5A; Table 1). In accordance with the reduced cell number, the expression of the cell division marker *CYCB1;1* (Colon-Carmona *et al.*, 1999) was restricted to a smaller region in the RAM of *sik1-4* (Fig. 5B).

Furthermore, reduced cell expansion was observed in *sik1-4* root hairs. In 7-day-old wild-type seedlings, root hairs have an average length of 250 μm, whereas in *sik1-4*, most root hairs were shorter than 200 μm, with an average length of 161 μm (Fig. 5C, D).

The fifth rosette leaf of 4-week-old *sik1-4* also had a much smaller area (47.8 mm^2 on average) than that of the wild type (165.9 mm^2 on average) (Fig. 5E; Table 1). The area of the lower epidermal pavement cell in *sik1-4* is on average 3271.5 μm^2, which is 37% of that of the wild type (8955.4 μm^2) (Fig. 5F; Table 1). The number of pavement cells in the fifth leaf of *sik1-4* was thus calculated to be 79% of that of the wild type. Petals of fully opened *sik1-4* flowers were also smaller than those of the wild type (1.00 mm^2 versus 1.85 mm^2) (Fig. 5G). The area of the petal cell in *sik1-4* is on average 191.0 μm^2, 87% of that of the wild type (220 μm^2 on average). The number of cells in the petal of *sik1-4* was calculated to be 62% of that of the wild type (Fig. 5H; Table 1). It appeared that the dwarf phenotype of *sik1-4* results from both reduced cell number and reduced cell size.

Reduced cell proliferation in a leaf can sometimes trigger cell expansion, leading to compensation phenotypes (Tsukaya, 2013). Since cell size is often correlated with endoreduplication (Massonnet *et al.*, 2011; Hepworth and Lenhard, 2014), flow cytometry analysis was performed on the fifth rosette leaf of 4-week-old plants to see if the smaller cell size in *sik1-4* was accompanied by a reduction in endoreduplication. Indeed, *sik1-4* has a lower ploidy level compared with the wild type (Fig. 5I).

Considering that SIK1 can complement the function of Ste20 in mitotic exit (Fig. 1D), *SIK1* promoter activity is mainly detected in non-dividing cells (Fig. 2), and that *sik1-4* has insufficient endoreduplication (Fig. 5I), we postulated that the SIK1 activity could be required for cell cycle exit in Arabidopsis. During Arabidopsis leaf development, cell proliferation mainly takes place at a very early stage (Andriankaja *et al.*, 2012), then the majority of cells exit the cell cycle abruptly. Therefore, we collected the first pair of true leaves on 8-, 11-, and 14-day-old seedlings and profiled the transcript levels of essential cell cycle genes and key regulators (*ANT* and *GRF5*) (Menges *et al.*, 2005; Yoshizumi

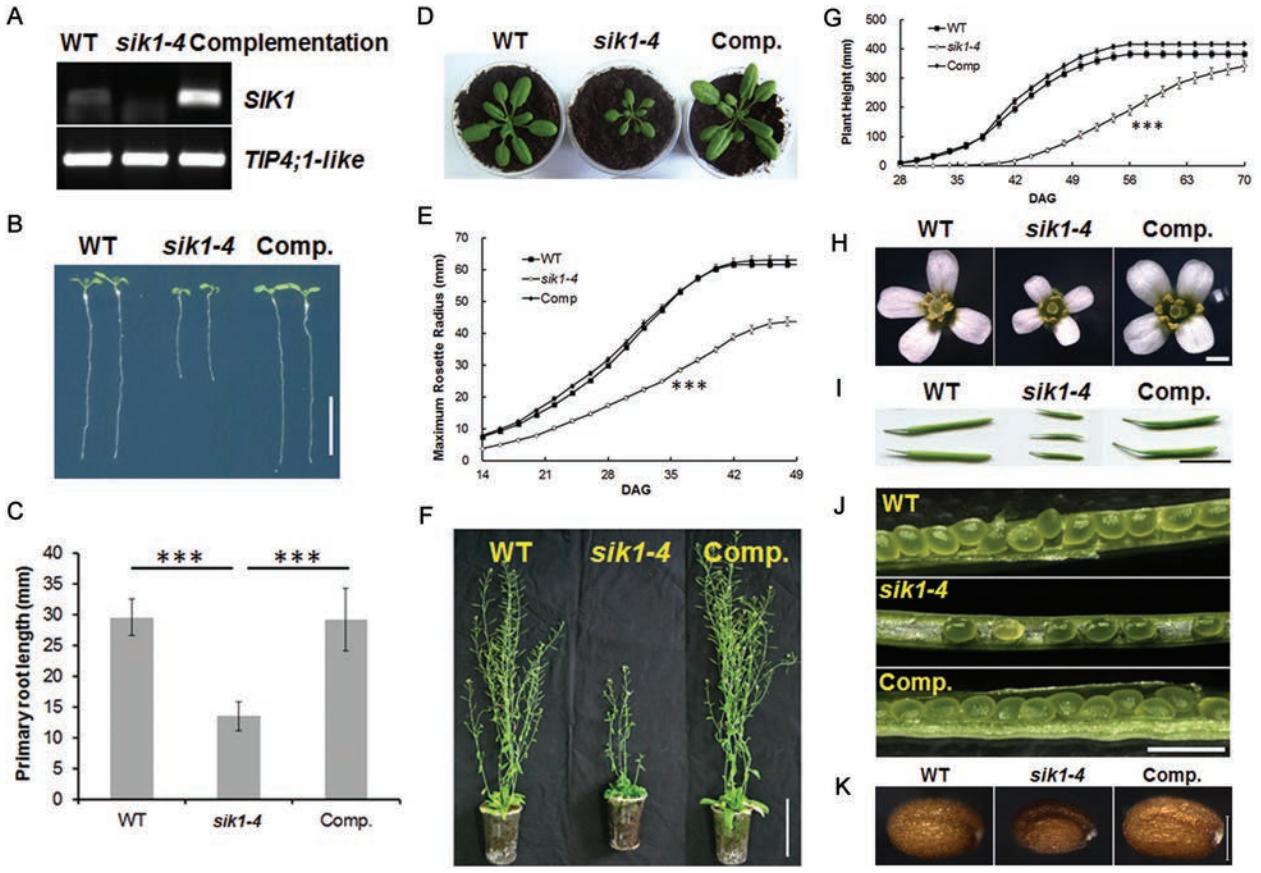

Fig. 4. Complementation of *sik1-4* with *pUBQ10:GFP-SIK1*. (A) Semi-quantitative RT-PCR of *SIK1* in the wild type, *sik1-4*, and the complementation (Comp.) line. *TIP4;1-like* is used as internal control. (B) Seven-day-old, vertically grown seedlings. (C) Quantification of primary root length of seedlings at 7 days post-germination (dpg). (D) Four-week-old plants. (E) Maximum rosette radii of the wild type, *sik1-1*, and the complementation line, measured over a period of 5 weeks. (F) Eight-week-old plants. (G) Plant height measured over a period of 6 weeks. (H) Fully opened flowers. (I) Mature siliques. (J) Halves of siliques. (K) Dry seeds. Bars=SE in (C), (E), and (G). *** indicates $P<0.001$ (Student's *t*-test) in (C), (E), and (G). Scale bars=1 cm in (B), (I), 10 cm in (F), 1 mm in (H), (J), 200 μm in (K). (This figure is available in colour at *JXB* online.)

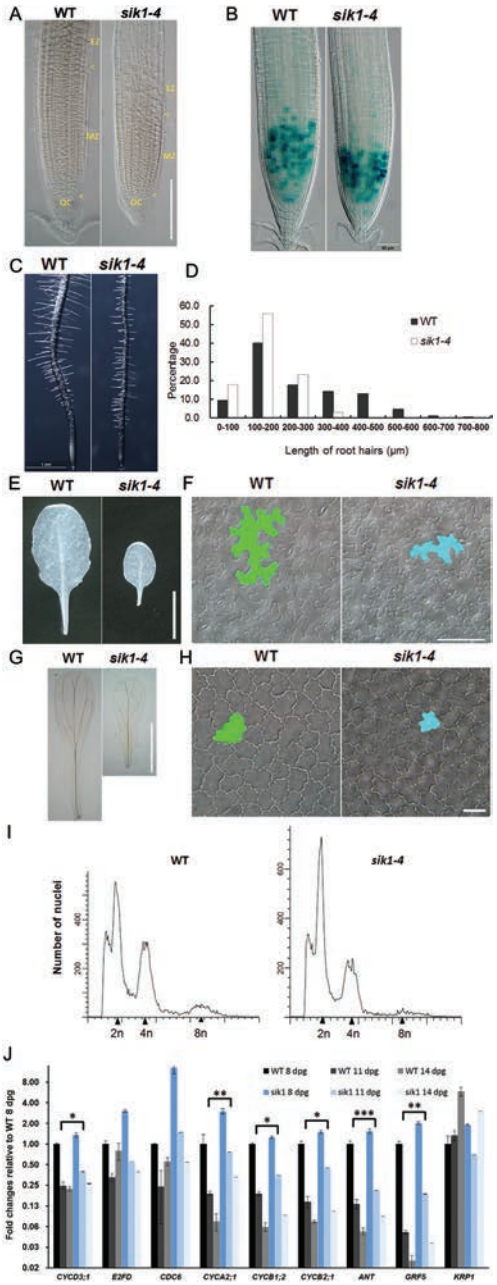

Fig. 5. *sik1-4* has reduced cell numbers, cell sizes, and ploidy levels compared with the wild type (WT). (A) Root tips of 6-day-old vertically grown WT and *sik1-4* seedlings. QC, quiescent center; MZ, meristematic zone; EZ, elongation zone. Arrows indicate the beginning of the MZ and EZ. (B) GUS staining showing *pCYCB1;1* promoter activity in WT and *sik1-4* root tips 7 days post-germination (dpg). (C) Root hairs (n >1000) of WT and *sik1-4* seedlings at 7 dpg. (D) Distribution of root hair lengths in the WT and *sik1-4*. (E) The fifth rosette leaves of the WT and *sik1-4* at 28 dpg. (F) Lower epidermis of (E) with representative cells highlighted. (G) Petals from fully opened flowers. (H) Lower epidermis of (G) with representative cells highlighted. (I) Flow cytometric analysis of the fifth rosette leaf of 28-day-old WT and *sik1-4*. A total of 20 000 nuclei are sorted for each sample. (J) Quantitative RT-PCR of core cell cycle marker genes and regulators from the first and second true leaves of 8-, 11-, and 14-day-old seedlings. *CYCD3;1*, G_1 phase-specific marker; *E2FD/DEL2*, G_1/S specific; *CDC6*, S-phase specific; *CYCA2;1*, S/G_2 specific; *CYCB1;2* and *CYCB2;1*, G_2/M-phase specific markers. *ANT* and *GRF5*, transcription factors that regulate cell proliferation; *KRP1*, cell cycle inhibitor. Bars=SD. *GAPC2* used as internal control. ***P<0.001, ** P<0.01, and *P<0.05 (Student's t-test) in (J). Scale bars=100 μm in (A), 50 μm in (B), (F); 1 mm in (C), (G); 1 cm in (E), 20 μm in (H). (This figure is available in colour at *JXB* online.)

et al., 2006; Andriankaja *et al.*, 2012). In the wild type, the cell cycle markers indeed had the highest transcript levels on day 8 and much lower transcript levels on days 11 and 14 (Fig. 5J). A similar trend was observed in *sik1-4*. However, at any given time point, the relative transcript levels of nearly all genes examined were higher in *sik1-4* than in the wild type. Consistently, expression of *KRP1*, the negative regulator of the cell cycle and promoter of endoreduplication (Schnittger *et al.*, 2003; Weinl *et al.*, 2005), was induced less in *sik1-4* compared with the wild type. These data suggested that SIK1 has a positive role in cell cycle exit.

MOB1A and MOB1B were identified as SIK1-interacting proteins

To gain more insights into SIK1 function, a Y2H screen was carried out using SIK1 as the bait. In total, sequences of 46 prey proteins were recovered from 266 positive clones (Supplementary Table S2). Among them, Mob1A (At5g45550) and Mob1B (At4g19045) were identified 212 times and six times, respectively. Since Mob1A and Mob1B have been well established as homologs of the kinase scaffold protein MOB (Citterio *et al.*, 2005, 2006), and as the reported phenotypes of the *mob1* T-DNA insertion mutant and RNAi lines are very similar to those of *sik1* (Galla *et al.*, 2011; Pinosa *et al.*, 2013), we postulated that SIK1 could be the kinase with which the Mob1s interact, and that the interaction might be important for their physiological functions.

SIK1 interacts with MOB1 at its N-terminal domain

To map the domains of SIK1 that mediate the interaction, SIK1 was subdivided into four fragments (Fig. 6A), and their abilities to interact with MOB1s were evaluated with Y2H. None of the BD constructs had self-activating activities (Fig. 6B), and on YEP medium without tryptophan and leucine (–Trp–Leu), all colonies developed normally (Fig. 6C). On –Trp–Leu–His plates, N1-SIK1 (amino acids 1–235), N-SIK1 (amino acids 1–504), and full-length SIK1 appeared as interacting with both MOB1A and MOB1B (Fig. 6C). On –Trp–Leu–His–Ade plates, only N-SIK1 and full-length SIK1 appeared to have strong interactions with MOB1s (Fig. 6C). Switching AD and BD domains between SIK1 and MOB1s gave consistent results (Fig. 6D). Unfortunately, SIK1, even in its kinase-dead form (K278R and D371A), was toxic to *Escherichia coli* (Supplementary Fig. S5), thus no *in vitro* pull-down results were obtained.

The interaction between SIK1 and MOB1A was hence further confirmed with BiFC in tobacco leaf epidermal cells. When SIK1–cEYFP was co-expressed with MOB1A–nEYFP, YFP signals were detected at, or in the vicinity of, the PM, and at punctate structures inside the cell (Fig. 6D). Interestingly, when N1-SIK1–cEYFP and MOB1A–nEYFP were co-expressed, strong YFP signals were detected both at the PM and in the nucleus (Fig. 6D).

Subcellular localization of SIK1 and MOB1A was then analyzed. Red fluorescent protein (RFP)–SIK1 partly co-localized with the *trans*-Golgi network/early endosome (TGN/EE)

Table 1. *sik1 has a lower cell number and reduced cell sizes compared with the wild type.*

Parameter	Wild type (average ±SE)	*sik1-4* (average ±SE)	Student's *t*-test
Length of RAM (μm), 7 dpg	296.6±4.2 (*n*=86)	182.8±2.5 (*n*=84)	*P*<1E-50
No. of protoderm cells in RAM, 7 dpg	38.2±0.4 (*n*=86)	24.0±0.3 (*n*=84)	*P*<1E-61
Length of RAM region with *pCYCB1;1:GUS* activity (μm)	186.8±2.5 (*n*=108)	116.1±2.1 (*n*=73)	*P*<1E-51
Area of petal (mm^2)	1.85±0.03 (*n*=123)	1.00±0.02 (*n*=109)	*P*<1E-61
Area of petal epidermal cell (μm^2)	220.8±2.7 (*n*=100)	191.0±2.8 (*n*=86)	*P*<1E-12
Area of the fifth rosette leaf, 28 dpg (mm^2)	165.9±7.2 (*n*=28)	47.8±3.4 (*n*=28)	*P*<1E-17
Area of lower epidermal cell (μm^2)	8955.4±121.9 (*n*=420)	3271.5±37.3 (*n*=440)	*P*<1E-99
No. of palisade cells per 250 000 μm^2	93.5±3.0 (*n*=43)	210.2±6.7 (*n*=44)	*P*<1E-23

dpg, days post-germination.

marker GFP–SYP43 (Uemura *et al.*, 2012) and the PM marker pm-gk (Nelson *et al.*, 2007) (Fig. 7A). Consistent with previous reports (Van Damme *et al.*, 2004; Galla *et al.*, 2011), nuclear localization of MOB1A was observed. In addition, MOB1A co-localized with the PM and the tonoplast (Fig. 7B). When co-expressed, SIK1 and MOB1A were co-localized not only at the PM but also in the nucleus (Fig. 7C). Furthermore, N1-SIK1 was localized to both the PM and the nucleus, and strongly co-localized with MOB1A in both compartments (Fig. 7D). These observations agree with the BiFC results and suggest that the N-terminal domain of SIK1 may be responsible for both MOB1A binding and the nuclear localization of SIK1.

Genetic analysis of SIK1 *and* MOB1A

Since SIK1 interacts with MOB1A, and their knock-out mutants have similar phenotypes, we further analyzed the genetic interaction between *SIK1* and *MOB1A*. First, *sik1-4* and *mob1a-1* (GABI_719G04) (Pinosa *et al.*, 2013) were crossed to generate *sik1 mob1a* double mutants. *sik1–/–mob1a+/–* had stronger phenotypes than *sik1* itself (Fig. 8A). In the progeny of *sik1–/–mob1a+/–*, approximately a quarter of the seeds failed to germinate or became arrested at growth stage 0.7–1.04 (Fig. 8A, B). These growth-arrested seedlings were confirmed as *sik1–/–mob1a–/–* by genomic PCR (data not shown). Then, a MOB1A-overexpression line (MOB1A-OE) and a SIK1-overexpression line (SIK1-OE) were generated and verified as functional by complementation of *mob1a* and *sik1* mutants, respectively (Fig. 4; Supplementary Fig. S6). The OE lines were then crossed into *sik1-1* and *mob1a-1*, respectively, to see if overexpression of either protein could rescue the deletion of the other (Fig. 8C–G). The resulting *sik1*/MOB1A-OE has phenotypes identical to *sik1*, and *mob1a*/SIK1-OE has phenotypes identical to *mob1a*. Our observations indicated that, similar to the metazoan Hippo pathway, other players are directly involved in SIK1- and MOB1A-mediated organ size control.

Discussion

The molecular function of Hippo is probably conserved among eukaryotes

Since its discovery (Harvey *et al.*, 2003; Jia *et al.*, 2003; Pantalacci *et al.*, 2003; Udan *et al.*, 2003; Wu *et al.*, 2003), the Hippo tumor suppressor pathway has been regarded as a central signaling pathway that controls metazoan organ growth (Pan, 2010; Yu and Guan, 2013). The core component—the STE20-like kinase Hippo—negatively regulates cell proliferation and promotes apoptosis (Rawat and Chernoff, 2015). Such molecular functions are shared by its yeast homologs. Ste20 has been shown to act as a sensor and master regulator of cell volume under various stress conditions (Strange *et al.*, 2006) and as a positive regulator of cell death (Ahn *et al.*, 2005). In addition, a recent systematic genetic screen has identified a negative regulatory role for Ste20 in cell size control, and established it as a node in a genetic network that links cell size control to cell polarity and mitotic exit (Soifer and Barkai, 2014). Another kinase that is closely related to the STE20 family, Cdc15, is a key component of the MEN pathway that mediates exit from mitosis (Rock *et al.*, 2013). In animals, the role of Cdc15 is known to be carried out by the MST kinases, which are also STE20 family members (Praskova *et al.*, 2008).

Although the Arabidopsis *sik1* null mutant is dwarf, it does not mean that SIK1 has an opposite function to Hippo. In fact, the *hpo* null mutants are lethal (Harvey *et al.*, 2003; Wu *et al.*, 2003) or growth arrested at the early third instar larvae stage (Shian Wu, personal communication). The dramatic tissue overgrowth phenotype was observed in the mosaic eyes and wing discs, in which cells homozygous for *hpo* maintain a higher proliferation rate over their neighboring wild-type cells (Harvey *et al.*, 2003; Jia *et al.*, 2003; Pantalacci *et al.*, 2003; Udan *et al.*, 2003; Wu *et al.*, 2003). Similarly, in developing young leaves, SIK1 appears to be required for the timely exit from the cell cycle and entry into endoreduplication and cell expansion, as suggested by GUS staining, Q-RT-PCR analysis, and flow cytometry. In animals, organ size is determined by cell proliferation and apoptosis; hence a mutation in mitotic exit leads to tissue overgrowth. In plants, however, organ size is determined by cell proliferation and (especially) subsequent cell expansion; hence the same mutation results in a dwarf plant. In summary, the function of Hippo in mitotic exit is probably conserved among eukaryotes.

A possible structural basis for the kinase–scaffold interaction

Now that we have confirmed the SIK1–MOB1 interaction in Arabidopsis, this interaction can be considered evolutionarily

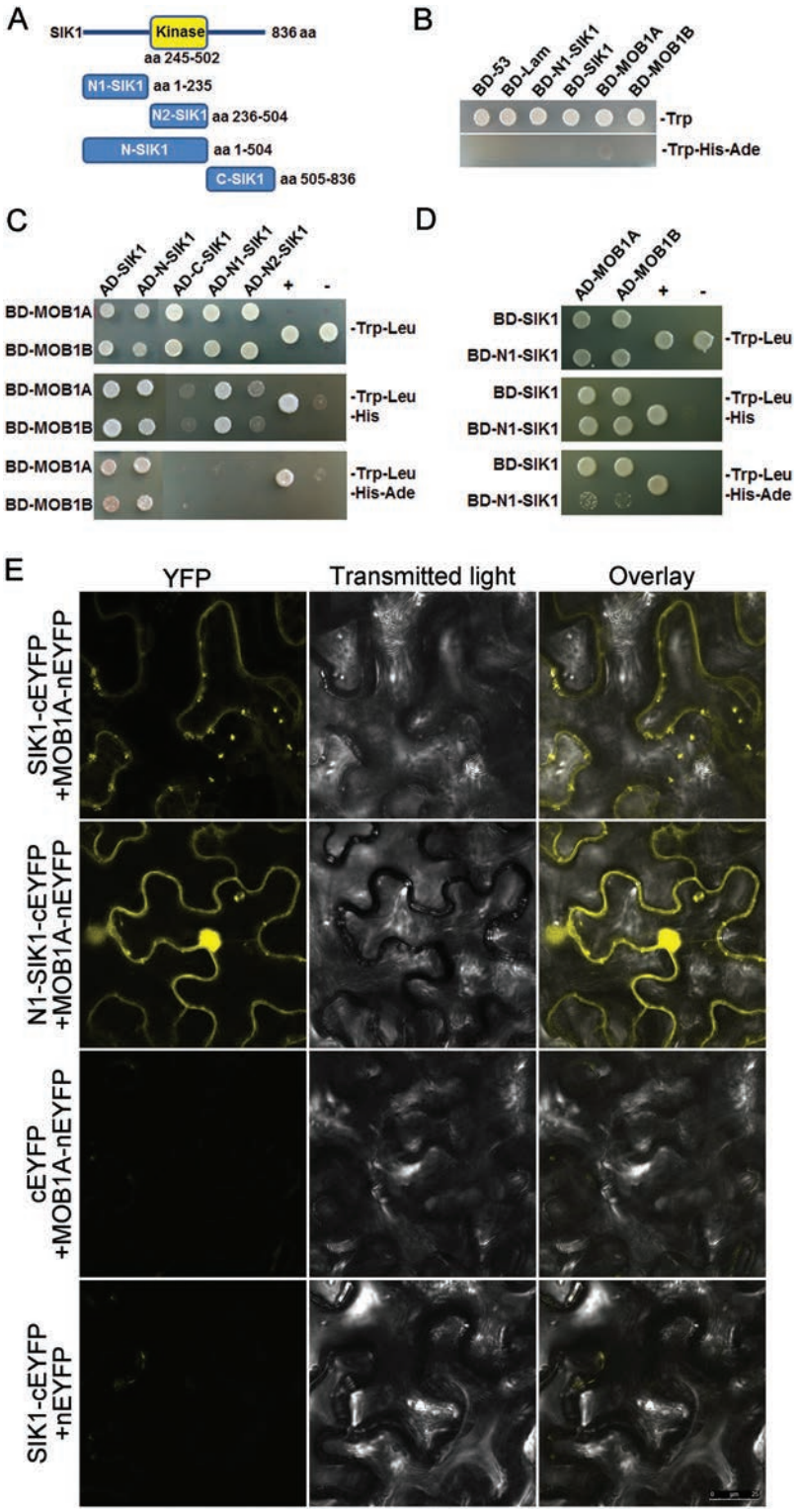

Fig. 6. The N-terminal domain of SIK1 (N1-SIK1) is responsible for its interaction with MOB1s. (A) SIK1 is subdivided into four fragments for yeast two-hybrid (Y2H) analysis. (B) SIK1 and MOB1s do not have self-activation activity. (C) Interaction between the full length and fragments of SIK1 (plus the activation domain, AD) and MOB1s (plus the binding domain, BD) verified on triple- and quadruple-dropout plates. + and –, positive and negative controls. (D) Interactions between AD-MOB1s and BD-SIK1. (E) Interaction between SIK1 and MOB1A confirmed in tobacco leaf epidermal cells with bimolecular fluorescence complementation (BiFC). Scale bar=50 μm in (E). (This figure is available in colour at *JXB* online.)

conserved among eukaryotes. The next questions to answer include how the interaction is achieved and regulated *in vivo*. We were surprised to see that the affinity towards MOB1 is mediated mainly by the N-terminal region of SIK1. Hippo/MSTs do not have such a region, and the N-terminal region of STE20 shares little homology with N1-SIK1 (Supplementary Fig. S2). Reported structures of human Mob1A and Mob1 from *Xenopus laevis* provided a plausible explanation

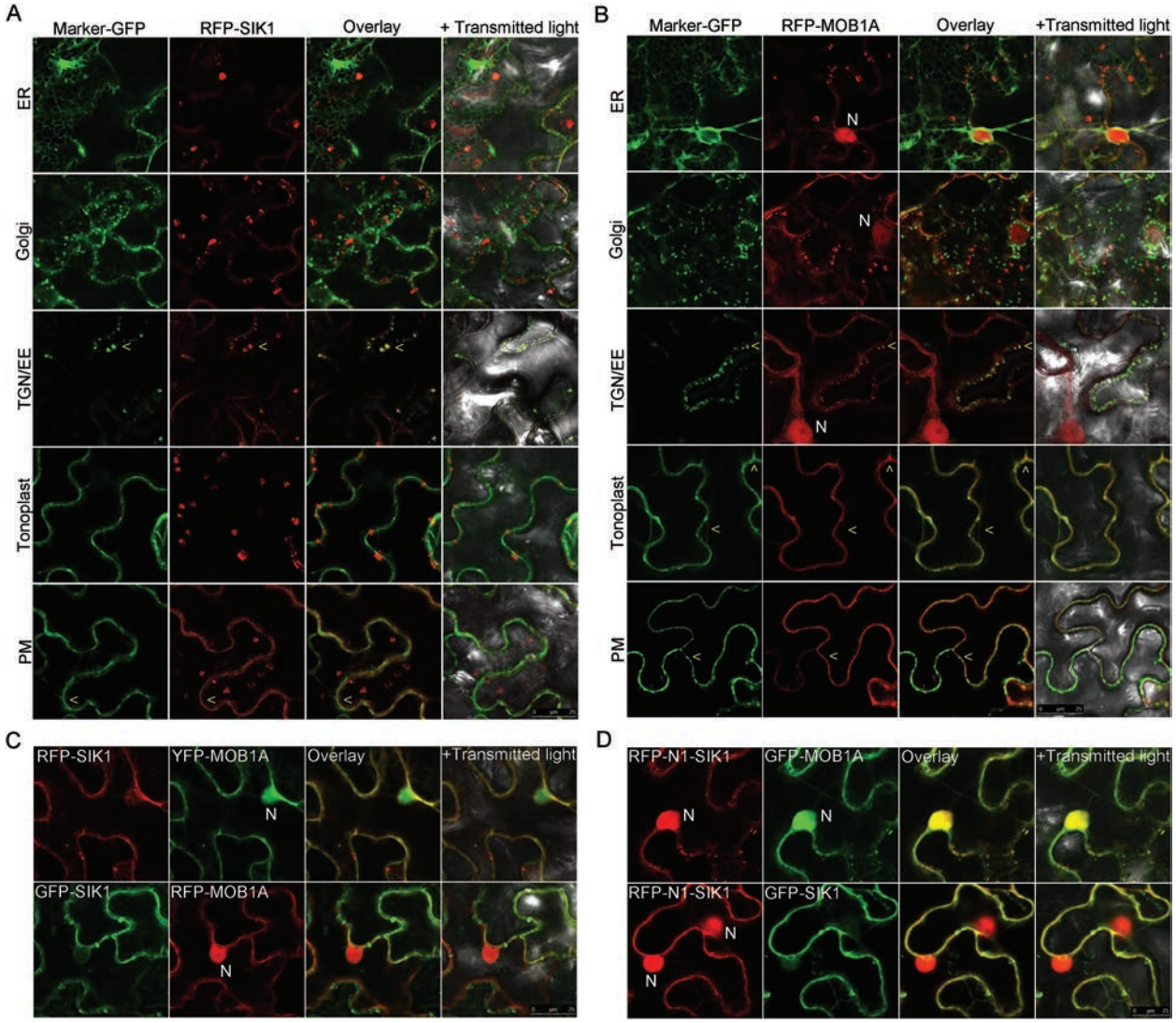

Fig. 7. Subcellular localization patterns of SIK1 and MOB1A. (A) RFP–SIK1 is co-expressed with GFP-tagged organelle markers. SIK1 is co-localized with *trans*-Golgi-network (TGN)/early endosome (EE) and plasma membrane (PM) markers. (B) RFP–MOB1A localizes to the nucleus (N), and co-localizes with TGN/EE, tonoplast, and PM markers. (C) When co-expressed with MOB1A, SIK1 can be detected in the nucleus (N). (D) N1-SIK1 localizes to the nucleus, and co-expression with N1-SIK1 brings SIK1 into the nucleus. Scale bars=25 μm in (A–D).

(Stavridi *et al.*, 2003; Ponchon *et al.*, 2004). The N-terminus of a helix (H2) and its adjacent loop (L1) of Mob1A form an evolutionarily conserved surface with a strong negative charge. Mutations in the conserved negatively charged amino acid residues, such as E51 and E55, have been shown to abolish Mob1A function (Stavridi *et al.*, 2003). Consistently, the yeast kinases that are known to interact with Mob1 homologs, such as Dbf2 and Cbk1 from budding yeast and Sid2 from fission yeast, all have a basic region at their N-terminal lobe (Stavridi *et al.*, 2003). The kinase–scaffold interaction has further been demonstrated to occur on the acidic, conserved surface of Mob1 and the N-terminal basic region of NDR kinase (Ponchon *et al.*, 2004). The Arabidopsis MOB1s are well conserved with hMob1A, especially at their N-termini (Ponchon *et al.*, 2004), with their 51 and 55 amino acid residues being glutamic acid as in hMob1A. Moreover, the N-terminal region of SIK1 is indeed enriched in basic amino acid residues. Hence SIK1 and MOB1 may also interact electrostatically with their charged surfaces.

How SIK1 may participate in organ size control

Previous studies and our observations showed that the *sik1* and *mob1* mutants share strikingly similar phenotypes, which is consistent with the fact that the two proteins have a strong interaction. Quantification of cell numbers and sizes in various organs, Q-RT-PCR of the cell division marker genes, and nuclear DNA content measurement all indicated that SIK1 (and MOB1) participates in both cell proliferation and cell expansion. The interaction between SIK1 and MOB1 thus should have a role in organ size control. Inside the cell, the subcellular localization patterns of SIK1 and MOB1, along with the BiFC results, indicated that the SIK1–MOB1 interaction happens mainly at the PM. The genetic analysis also implied that SIK1 and MOB1 are components of a larger complex that mediates cell cycle progression and organ growth. It could be postulated that an as yet unknown upstream signal induces SIK1–MOB1 interaction at the PM, and the downstream signaling cascade may involve events that take place

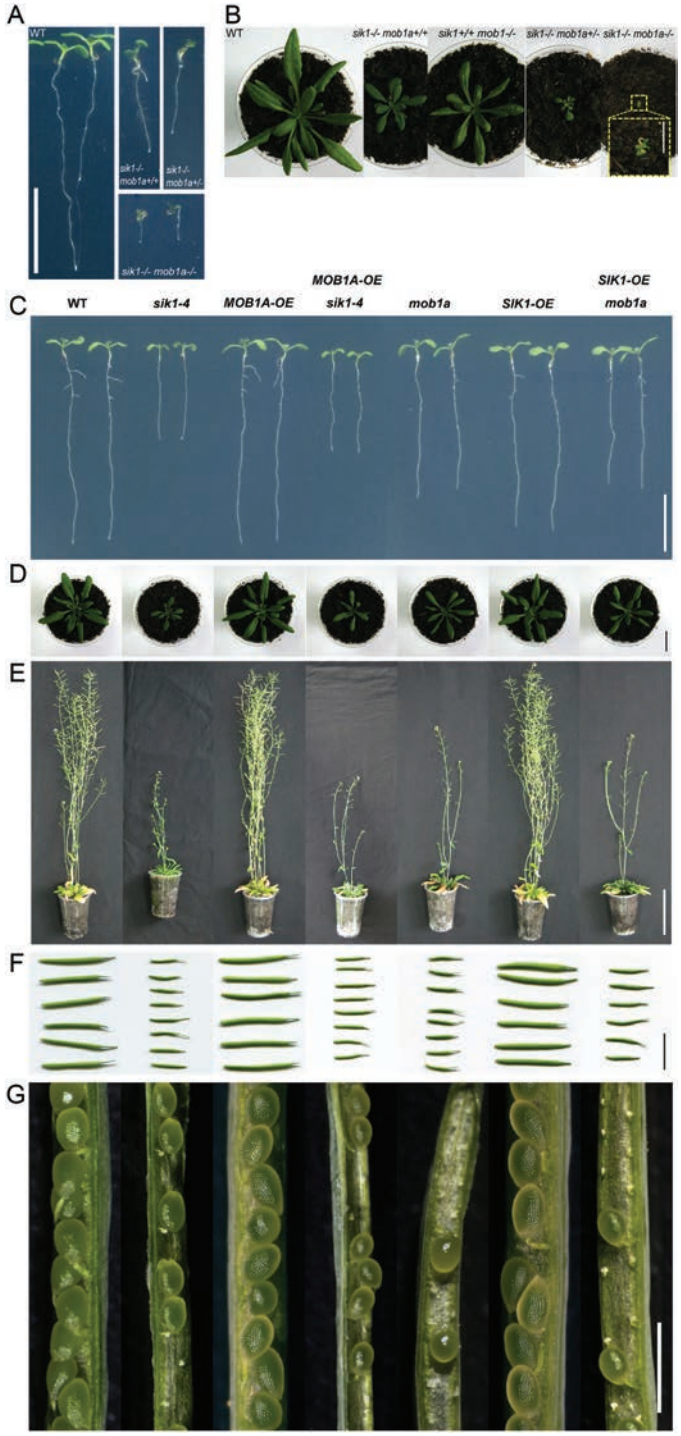

Fig. 8. Genetic interactions between *SIK1* and *MOB1A*. (A) Ten-day-old *sik1–/– mob1a+/–* has more severe phenotypes than *sik1* alone, and *sik1–/–mob1a–/–* is growth arrested. (B) The same phenotypes are observed on 4-week-old, soil-grown plants. (C) The 10-day-old transgenic line carrying *35S:MOB1A* in the *sik1-4* background has the same phenotypes as *sik1-4*. *35S:SIK1* can also not rescue *mob1a*. (D–G) Phenotypes consistent with (C) are observed in (D) 4-week-old, soil-grown plants; (E) 8-week-old plants; (F) mature siliques; (G) halves of siliques. Scale bars=1 cm in (A), (B) (by the double mutant), (C), (D), (F); 10 cm in (E); 1 mm in (G). (This figure is available in colour at *JXB* online.)

in the nucleus. In *Drosophila*, localization of Mats at the PM is critical for its activation and thus inhibition of tissue growth (Ho *et al.*, 2010). However, Hippo itself has not been reported to shuttle between the cytoplasm and the nucleus. It was the essential downstream component of the Hippo pathway—the transcriptional co-activator Yap/Yorkie—that shuttles (Huang *et al.*, 2005). Phosphorylation of Yap by Wts leads to sequestration of Yap in the cytoplasm and thus suppression of the transcription mediated by Yap and Sd/TEAD transcription factors (Zhao *et al.*, 2010). De-phosphorylation of Yap, in contrast, leads to its translocation into the nucleus and subsequent activation of Sd/TEADs, to induce transcription (Zhao *et al.*, 2010). It is therefore safe to say that the plant pathway differs from the metazoan one.

Although the plant SIK1 pathway is far from complete, clues can be found on how SIK1 may participate in organ size control. First, our Y2H screen identified interesting potential interacting partners for SIK1 (Supplementary Table S3). Among these proteins is the Rho-family GTPase ROP6, an essential regulator of cortical microtubule ordering and cell expansion (Fu *et al.*, 2009). As a CDC42 homolog, it was somewhat expected that ROP6 would interact with SIK1, yet the lack of a CRIB domain in SIK1 suggests that the ROP6–SIK1 interaction should have a different structural basis from that of the CDC42–STE20 interaction. Several other potential SIK1-interacting proteins are regulators of vesicular trafficking and polarity establishment, such as CHMP1A/VPS46.2 (Spitzer *et al.*, 2009) and PIPK11 (Ischebeck *et al.*, 2011). Such an observation is consistent with the fact that SIK1 can be found at the TGN/EE, where trafficking routes converge. Considering that polarity establishment and directional growth of plant cells have been largely associated with intracellular trafficking processes (Reyes *et al.*, 2011), a function for SIK1 in trafficking is possibly not unexpected and worthy of future investigation. Another clue came from a preliminary microarray analysis. Whereas no significantly enriched (with $e<10^{-5}$) Gene Ontology (GO) terms were identified from the top 400 (5%) genes that have higher transcript levels in *sik1*, the top 400 genes with lower transcript levels in *sik1* were enriched in GO terms such as response to biotic stimulus (7.24e-15), defense response (5.32e-12), response to oxidative stress (2.42e-9), and, very interestingly, response to jasmonic acid (JA) stimulus (6.18e-10). Genes encoding jasmonate-ZIM-domain (JAZ) proteins were among the most strongly repressed genes in *sik1*. We verified the observation with Q-RT-PCR. Indeed, in both *sik1* and *mob1a*, all *JAZ* genes examined, along with *MYC2*, *MYC3*, and *MYC4*, had significantly lower transcript levels than in the wild type (Supplementary Fig. S7). Since JAZs are JA co-receptors and transcriptional repressors (Thines *et al.*, 2007), and since transcription of both JAZs and MYCs has been shown to be co-ordinately regulated (Chung *et al.*, 2008), it can be postulated that *sik1* (and possibly also *mob1a*) tries to tune down the JA signaling pathway to loosen the strain on cell division and cell expansion generated by loss of *SIK1* gene function. Whether SIK1 directly participates in JA signaling remains to be elucidated.

In conclusion, a Hippo/STE20 homolog was for the first time identified and characterized as a regulator of organ size in plants, with its scaffold proteins revealed through a screen and the molecular basis for their interaction explored. Currently,

the pathway is far from complete, since two essential components, Warts and Salvador, remain unidentified. Furthermore, the *sik1* null mutant is not lethal, and, despite a likely function of SIK1 in mitotic exit, mature organs of *sik1* have fewer cell numbers. There are several possible reasons for such contradictory observations. First, non-cell-autonomous signaling events are clearly involved in organ size determination in *sik1*. It is also possible that *sik1* has a slower cell division rate, or it may have smaller primordium initials, or fewer dispersed divisions after mitotic exit. In fact, the transcript levels of cell division markers are lower in the fifth rosette leaf of 4-week-old *sik1* compared with the wild type (Supplementary Fig. S8), indicating that dispersed division after the mitotic exit could be less in *sik1*. Further studies are necessary to elucidate how SIK1 may participate in organ size control. Nevertheless, this study lays a foundation for future construction of a complete plant Hippo/STE20 pathway, which will enhance our understanding of how core signaling pathways may evolve and adapt differently in animals and plants.

Supplementary data

Supplementary data are available at *JXB* online.

Figure S1. Splicing variant *At1g69220.1* is the major form of *SIK1* transcript.

Figure S2. The N-terminal region of SIK1 shares little homology with other Ste20 family members.

Figure S3. Details of GUS staining of 10-day-old transgenic plants carrying *pSIK1:GUS* and *SIK1:GUS*.

Figure S4. Transgenic lines carrying *35S:GFP-SIK1* are comparable with the control in size.

Figure S5. SIK1 expression induced cell death in *E. coli*.

Figure S6. Complementation of *mob1a* with a MOB1A overexpression line.

Figure S7. JAZs and MYCs have much lower mRNA levels in *sik1* and *mob1* than in the wild type.

Figure S8. Quantitative RT-PCR of core cell cycle marker genes from the fifth rosette leaves of 28-day-old plants.

Table S1. Primers used in this study.

Table S2. SIK1-interacting proteins identified in yeast two-hybrid screen.

Table S3. Growth parameters of *sik1-4*, the wild type, and the complementation line.

Acknowledgements

We thank the Arabidopsis Biological Resource Center (ABRC), Drs Peter Doerner, Yule Liu, and Zhiping Xie for seeds, yeast strains, and vectors; Drs Shian Wu and Zhiping Xie for critical reading of the manuscript; and Drs Shuzhen Men, Shifeng Zhu, Zhiping Xie, and our lab members for discussions. This work was supported by the National Key Basic Research Program of China (2011CB910100), the National Natural Science Foundation of China (30970251, 31401179), and the Tianjin Research Program of Applied Basic and Cutting-edge Technologies (No. 11JCZDJC16400).

References

Ahn SH, Cheung WL, Hsu JY, Diaz RL, Smith MM, Allis CD. 2005. Sterile 20 kinase phosphorylates histone H2B at serine 10 during hydrogen peroxide-induced apoptosis in S. cerevisiae. Cell **120,** 25–36.

Alonso JM, Stepanova AN, Leisse TJ, *et al*. 2003. Genome-wide insertional mutagenesis of Arabidopsis thaliana. Science **301,** 653–657.

Andriankaja M, Dhondt S, De Bodt S, *et al*. 2012. Exit from proliferation during leaf development in Arabidopsis thaliana: a not-so-gradual process. Developmental Cell **22,** 64–78.

Bardwell L. 2005. A walk-through of the yeast mating pheromone response pathway. Peptides **26,** 339–350.

Bartholomew CR, Hardy CF. 2009. p21-activated kinases Cla4 and Ste20 regulate vacuole inheritance in Saccharomyces cerevisiae. Eukaryotic Cell **8,** 560–572.

Blomme J, Inze D, Gonzalez N. 2014. The cell-cycle interactome: a source of growth regulators? Journal of Experimental Botany **65,** 2715–2730.

Boyce KJ, Andrianopoulos A. 2011. Ste20-related kinases: effectors of signaling and morphogenesis in fungi. Trends in Microbiology **19,** 400–410.

Brioudes F, Thierry AM, Chambrier P, Mollereau B, Bendahmane M. 2010. Translationally controlled tumor protein is a conserved mitotic growth integrator in animals and plants. Proceedings of the National Academy of Sciences, USA **107,** 16384–16389.

Cho HT, Cosgrove DJ. 2000. Altered expression of expansin modulates leaf growth and pedicel abscission in Arabidopsis thaliana. Proceedings of the National Academy of Sciences, USA **97,** 9783–9788.

Chung HS, Koo AJ, Gao X, Jayanty S, Thines B, Jones AD, Howe GA. 2008. Regulation and function of Arabidopsis JASMONATE ZIM-domain genes in response to wounding and herbivory. Plant Physiology **146,** 952–964.

Citterio S, Albertini E, Varotto S, Feltrin E, Soattin M, Marconi G, Sgorbati S, Lucchin M, Barcaccia G. 2005. Alfalfa Mob 1-like genes are expressed in reproductive organs during meiosis and gametogenesis. Plant Molecular Biology **58,** 789–807.

Citterio S, Piatti S, Albertini E, Aina R, Varotto S, Barcaccia G. 2006. Alfalfa Mob1-like proteins are involved in cell proliferation and are localized in the cell division plane during cytokinesis. Experimental Cell Research **312,** 1050–1064.

Clough SJ, Bent AF. 1998. Floral dip: a simplified method for Agrobacterium-mediated transformation of Arabidopsis thaliana. The Plant Journal **16,** 735–743.

Colon-Carmona A, You R, Haimovitch-Gal T, Doerner P. 1999. Technical advance: spatio-temporal analysis of mitotic activity with a labile cyclin–GUS fusion protein. The Plant Journal **20,** 503–508.

Dan I, Watanabe NM, Kusumi A. 2001. The Ste20 group kinases as regulators of MAP kinase cascades. Trends in Cell Biology **11,** 220–230.

Deprost D, Yao L, Sormani R, Moreau M, Leterreux G, Nicolai M, Bedu M, Robaglia C, Meyer C. 2007. The Arabidopsis TOR kinase links plant growth, yield, stress resistance and mRNA translation. EMBO Reports **8,** 864–870.

Disch S, Anastasiou E, Sharma VK, Laux T, Fletcher JC, Lenhard M. 2006. The E3 ubiquitin ligase BIG BROTHER controls arabidopsis organ size in a dosage-dependent manner. Current Biology **16,** 272–279.

Drogen F, O'Rourke SM, Stucke VM, Jaquenoud M, Neiman AM, Peter M. 2000. Phosphorylation of the MEKK Ste11p by the PAK-like kinase Ste20p is required for MAP kinase signaling in vivo. Current Biology **10,** 630–639.

Du L, Li N, Chen L, Xu Y, Li Y, Zhang Y, Li C, Li Y. 2014. The ubiquitin receptor DA1 regulates seed and organ size by modulating the stability of the ubiquitin-specific protease UBP15/SOD2 in Arabidopsis. The Plant Cell **26,** 665–677.

Eswaran J, Soundararajan M, Kumar R, Knapp S. 2008. UnPAKing the class differences among p21-activated kinases. Trends in Biochemical Sciences **33,** 394–403.

Feng G, Qin Z, Yan J, Zhang X, Hu Y. 2011. Arabidopsis ORGAN SIZE RELATED1 regulates organ growth and final organ size in orchestration with ARGOS and ARL. New Phytologist **191,** 635–646.

Fu Y, Xu T, Zhu L, Wen M, Yang Z. 2009. A ROP GTPase signaling pathway controls cortical microtubule ordering and cell expansion in Arabidopsis. Current Biology **19,** 1827–1832.

Galbraith DW, Harkins KR, Maddox JM, Ayres NM, Sharma DP, Firoozabady E. 1983. Rapid flow cytometric analysis of the cell cycle in intact plant tissues. Science **220,** 1049–1051.

Galla G, Zenoni S, Marconi G, *et al*. 2011. Sporophytic and gametophytic functions of the cell cycle-associated Mob1 gene in Arabidopsis thaliana L. Gene **484,** 1–12.

Goh HH, Sloan J, Dorca-Fornell J, Fleming A. 2012. Inducible repression of multiple expansin genes leads to growth suppression during leaf development. Plant Physiology **159,** 1759–1770.

Gonzalez N, Vanhaeren H, Inze D. 2012. Leaf size control: complex coordination of cell division and expansion. Trends in Plant Science **17,** 332–340.

Harris K, Lamson RE, Nelson B, Hughes TR, Marton MJ, Roberts CJ, Boone C, Pryciak PM. 2001. Role of scaffolds in MAP kinase pathway specificity revealed by custom design of pathway-dedicated signaling proteins. Current Biology **11,** 1815–1824.

Harvey K, Tapon N. 2007. The Salvador–Warts–Hippo pathway—an emerging tumour-suppressor network. Nature Reviews Cancer **7,** 182–191.

Harvey KF, Pfleger CM, Hariharan IK. 2003. The Drosophila Mst ortholog, hippo, restricts growth and cell proliferation and promotes apoptosis. Cell **114,** 457–467.

Hepworth J, Lenhard M. 2014. Regulation of plant lateral-organ growth by modulating cell number and size. Current Opinion in Plant Biology **17,** 36–42.

Ho LL, Wei XM, Shimizu T, Lai ZC. 2010. Mob as tumor suppressor is activated at the cell membrane to control tissue growth and organ size in Drosophila. Developmental Biology **337,** 274–283.

Hofken T, Schiebel E. 2002. A role for cell polarity proteins in mitotic exit. EMBO Journal **21,** 4851–4862.

Hu Y, Poh HM, Chua NH. 2006. The Arabidopsis ARGOS-LIKE gene regulates cell expansion during organ growth. The Plant Journal **47,** 1–9.

Hu Y, Xie Q, Chua NH. 2003. The Arabidopsis auxin-inducible gene ARGOS controls lateral organ size. The Plant Cell **15,** 1951–1961.

Huang J, Wu S, Barrera J, Matthews K, Pan D. 2005. The Hippo signaling pathway coordinately regulates cell proliferation and apoptosis by inactivating Yorkie, the Drosophila homolog of YAP. Cell **122,** 421–434.

Ischebeck T, Stenzel I, Hempel F, Jin X, Mosblech A, Heilmann I. 2011. Phosphatidylinositol-4,5-bisphosphate influences Nt-Rac5-mediated cell expansion in pollen tubes of Nicotiana tabacum. The Plant Journal **65,** 453–468.

Jia J, Zhang W, Wang B, Trinko R, Jiang J. 2003. The Drosophila Ste20 family kinase dMST functions as a tumor suppressor by restricting cell proliferation and promoting apoptosis. Genes and Development **17,** 2514–2519.

Jonak C, Okresz L, Bogre L, Hirt H. 2002. Complexity, cross talk and integration of plant MAP kinase signalling. Current Opinion in Plant Biology **5,** 415–424.

Karpov PA, Nadezhdina ES, Yemets AI, Matusov VG, Nyporko AY, Shashina NY, Blume YB. 2010. Bioinformatic search of plant microtubule- and cell cycle related serine-threonine protein kinases. BMC Genomics **11** Suppl 1, S14.

Krizek BA. 1999. Ectopic expression of AINTEGUMENTA in Arabidopsis plants results in increased growth of floral organs. Developmental Genetics **25,** 224–236.

Krizek BA. 2009. Making bigger plants: key regulators of final organ size. Current Opinion in Plant Biology **12,** 17–22.

Kurepa J, Wang S, Li Y, Zaitlin D, Pierce AJ, Smalle JA. 2009. Loss of 26S proteasome function leads to increased cell size and decreased cell number in Arabidopsis shoot organs. Plant Physiology **150,** 178–189.

Lamson RE, Winters MJ, Pryciak PM. 2002. Cdc42 regulation of kinase activity and signaling by the yeast p21-activated kinase Ste20. Molecular and Cellular Biology **22,** 2939–2951.

Leeuw T, Wu C, Schrag JD, Whiteway M, Thomas DY, Leberer E. 1998. Interaction of a G-protein beta-subunit with a conserved sequence in Ste20/PAK family protein kinases. Nature **391,** 191–195.

Li Y, Zheng L, Corke F, Smith C, Bevan MW. 2008. Control of final seed and organ size by the DA1 gene family in Arabidopsis thaliana. Genes and Development **22,** 1331–1336.

Lin M, Unden H, Jacquier N, Schneiter R, Just U, Hofken T. 2009. The Cdc42 effectors Ste20, Cla4, and Skm1 down-regulate the expression of genes involved in sterol uptake by a mitogen-activated protein kinase-independent pathway. Molecular Biology of the Cell **20,** 4826–4837.

Liu D, Gong Q, Ma Y, *et al*. 2010. cpSecA, a thylakoid protein translocase subunit, is essential for photosynthetic development in Arabidopsis. Journal of Experimental Botany **61,** 1655–1669.

Liu Y, Schiff M, Czymmek K, Talloczy Z, Levine B, Dinesh-Kumar SP. 2005. Autophagy regulates programmed cell death during the plant innate immune response. Cell **121,** 567–577.

Martin-Trillo M, Cubas P. 2010. TCP genes: a family snapshot ten years later. Trends in Plant Science **15,** 31–39.

Massonnet C, Tisne S, Radziejwoski S, Vile D, De Veylder L, Dauzat M, Granier C. 2011. New insights into the control of endoreduplication: endoreduplication could be driven by organ growth in Arabidopsis leaves. Plant Physiology **157,** 2044–2055.

Menges M, de Jager SM, Gruissem W, Murray JA. 2005. Global analysis of the core cell cycle regulators of Arabidopsis identifies novel genes, reveals multiple and highly specific profiles of expression and provides a coherent model for plant cell cycle control. The Plant Journal **41,** 546–566.

Mizukami Y, Fischer RL. 2000. Plant organ size control: AINTEGUMENTA regulates growth and cell numbers during organogenesis. Proceedings of the National Academy of Sciences, USA **97,** 942–947.

Nelson BK, Cai X, Nebenfuhr A. 2007. A multicolored set of in vivo organelle markers for co-localization studies in Arabidopsis and other plants. The Plant Journal **51,** 1126–1136.

Nemoto K, Seto T, Takahashi H, Nozawa A, Seki M, Shinozaki M, Endo Y, Sawasaki T. 2011. Autophosphorylation profiling of Arabidopsis protein kinases using the cell-free system. Phytochemistry **72,** 1136–1144.

Omidbakhshfard MA, Proost S, Fujikura U, Mueller-Roeber B. 2015. Growth-regulating factors (GRFs): a small transcription factor family with important functions in plant biology. Molecular Plant **8,** 998–1010.

Pan D. 2010. The hippo signaling pathway in development and cancer. Developmental Cell **19,** 491–505.

Pantalacci S, Tapon N, Leopold P. 2003. The Salvador partner Hippo promotes apoptosis and cell-cycle exit in Drosophila. Nature Cell Biology **5,** 921–927.

Pinosa F, Begheldo M, Pasternak T, Zermiani M, Paponov IA, Dovzhenko A, Barcaccia G, Ruperti B, Palme K. 2013. The Arabidopsis thaliana Mob1A gene is required for organ growth and correct tissue patterning of the root tip. Annals of Botany **112,** 1803–1814.

Ponchon L, Dumas C, Kajava AV, Fesquet D, Padilla A. 2004. NMR solution structure of Mob1, a mitotic exit network protein and its interaction with an NDR kinase peptide. Journal of Molecular Biology **337,** 167–182.

Powell AE, Lenhard M. 2012. Control of organ size in plants. Current Biology **22,** R360–367.

Praskova M, Xia F, Avruch J. 2008. MOBKL1A/MOBKL1B phosphorylation by MST1 and MST2 inhibits cell proliferation. Current Biology **18,** 311–321.

Raitt DC, Posas F, Saito H. 2000. Yeast Cdc42 GTPase and Ste20 PAK-like kinase regulate Sho1-dependent activation of the Hog1 MAPK pathway. EMBO Journal **19,** 4623–4631.

Rawat SJ, Chernoff J. 2015. Regulation of mammalian Ste20 (Mst) kinases. Trends in Biochemical Sciences **40,** 149–156.

Reyes FC, Buono R, Otegui MS. 2011. Plant endosomal trafficking pathways. Current Opinion in Plant Biology **14,** 666–673.

Roberts RL, Fink GR. 1994. Elements of a single MAP kinase cascade in Saccharomyces cerevisiae mediate two developmental programs in the same cell type: mating and invasive growth. Genes and Development **8,** 2974–2985.

Rock JM, Lim D, Stach L, *et al*. 2013. Activation of the yeast Hippo pathway by phosphorylation-dependent assembly of signaling complexes. Science **340,** 871–875.

Sablowski R, Carnier Dornelas M. 2014. Interplay between cell growth and cell cycle in plants. Journal of Experimental Botany **65,** 2703–2714.

Schnittger A, Weinl C, Bouyer D, Schobinger U, Hulskamp M. 2003. Misexpression of the cyclin-dependent kinase inhibitor ICK1/KRP1 in single-celled Arabidopsis trichomes reduces endoreduplication and cell size and induces cell death. The Plant Cell **15,** 303–315.

Schruff MC, Spielman M, Tiwari S, Adams S, Fenby N, Scott RJ. 2006. The AUXIN RESPONSE FACTOR 2 gene of Arabidopsis links auxin signalling, cell division, and the size of seeds and other organs. Development **133,** 251–261.

Sessions A, Burke E, Presting G, *et al*. 2002. A high-throughput Arabidopsis reverse genetics system. The Plant Cell **14,** 2985–2994.

Sheu YJ, Barral Y, Snyder M. 2000. Polarized growth controls cell shape and bipolar bud site selection in Saccharomyces cerevisiae. Molecular and Cellular Biology **20,** 5235–5247.

Soifer I, Barkai N. 2014. Systematic identification of cell size regulators in budding yeast. Molecular Systems Biology **10,** 761.

Sonoda Y, Sako K, Maki Y, Yamazaki N, Yamamoto H, Ikeda A, Yamaguchi J. 2009. Regulation of leaf organ size by the Arabidopsis RPT2a 19S proteasome subunit. The Plant Journal **60,** 68–78.

Spitzer C, Reyes FC, Buono R, Sliwinski MK, Haas TJ, Otegui MS. 2009. The ESCRT-related CHMP1A and B proteins mediate multivesicular body sorting of auxin carriers in Arabidopsis and are required for plant development. The Plant Cell **21,** 749–766.

Stavridi ES, Harris KG, Huyen Y, Bothos J, Verwoerd PM, Stayrook SE, Pavletich NP, Jeffrey PD, Luca FC. 2003. Crystal structure of a human Mob1 protein: toward understanding Mob-regulated cell cycle pathways. Structure **11,** 1163–1170.

Strange K, Denton J, Nehrke K. 2006. Ste20-type kinases: evolutionarily conserved regulators of ion transport and cell volume. Physiology **21,** 61–68.

Thines B, Katsir L, Melotto M, Niu Y, Mandaokar A, Liu G, Nomura K, He SY, Howe GA, Browse J. 2007. JAZ repressor proteins are targets of the SCF(COI1) complex during jasmonate signalling. Nature **448,** 661–665.

Tsukaya H. 2013. Leaf development. The Arabidopsis Book **11,** e0163.

Udan RS, Kango-Singh M, Nolo R, Tao C, Halder G. 2003. Hippo promotes proliferation arrest and apoptosis in the Salvador/Warts pathway. Nature Cell Biology **5,** 914–920.

Uemura T, Kim H, Saito C, Ebine K, Ueda T, Schulze-Lefert P, Nakano A. 2012. Qa-SNAREs localized to the trans-Golgi network regulate multiple transport pathways and extracellular disease resistance in plants. Proceedings of the National Academy of Sciences, USA **109,** 1784–1789.

Van Damme D, Bouget FY, Van Poucke K, Inze D, Geelen D. 2004. Molecular dissection of plant cytokinesis and phragmoplast structure: a survey of GFP-tagged proteins. The Plant Journal **40,** 386–398.

Weinl C, Marquardt S, Kuijt SJ, Nowack MK, Jakoby MJ, Hulskamp M, Schnittger A. 2005. Novel functions of plant cyclin-dependent kinase inhibitors, ICK1/KRP1, can act non-cell-autonomously and inhibit entry into mitosis. The Plant Cell **17,** 1704–1722.

Wu S, Huang J, Dong J, Pan D. 2003. hippo encodes a Ste-20 family protein kinase that restricts cell proliferation and promotes apoptosis in conjunction with salvador and warts. Cell **114,** 445–456.

Wuyts N, Dhondt S, Inze D. 2015. Measurement of plant growth in view of an integrative analysis of regulatory networks. Current Opinion in Plant Biology **25,** 90–97.

Xia T, Li N, Dumenil J, Li J, Kamenski A, Bevan MW, Gao F, Li Y. 2013. The ubiquitin receptor DA1 interacts with the E3 ubiquitin ligase DA2 to regulate seed and organ size in Arabidopsis. The Plant Cell **25,** 3347–3359.

Xia T, Xiao D, Liu D, Chai W, Gong Q, Wang NN. 2012. Heterologous expression of ATG8c from soybean confers tolerance to nitrogen deficiency and increases yield in Arabidopsis. PLoS One **7,** e37217.

Xiong Y, McCormack M, Li L, Hall Q, Xiang C, Sheen J. 2013. Glucose–TOR signalling reprograms the transcriptome and activates meristems. Nature **496,** 181–186.

Yoshizumi T, Tsumoto Y, Takiguchi T, Nagata N, Yamamoto YY, Kawashima M, Ichikawa T, Nakazawa M, Yamamoto N, Matsui M. 2006. Increased level of polyploidy1, a conserved repressor of CYCLINA2 transcription, controls endoreduplication in Arabidopsis. The Plant Cell **18,** 2452–2468.

Yu FX, Guan KL. 2013. The Hippo pathway: regulators and regulations. Genes and Development **27,** 355–371.

Zenoni S, Fasoli M, Tornielli GB, Dal Santo S, Sanson A, de Groot P, Sordo S, Citterio S, Monti F, Pezzotti M. 2011. Overexpression of PhEXPA1 increases cell size, modifies cell wall polymer composition and affects the timing of axillary meristem development in Petunia hybrida. New Phytologist **191,** 662–677.

Zhao B, Li L, Lei Q, Guan KL. 2010. The Hippo–YAP pathway in organ size control and tumorigenesis: an updated version. Genes and Development **24,** 862–874.